A Theoretical Analysis of the Coupling of Light to Surface-Plasmon Oscillations at the Edge of a Slab Waveguide

Eduardo Fontana

***Abstract*— A theoretical method that accounts for diffraction and backcoupling of surface plasmon (SP) oscillations excited at the metallized edge of a planar waveguide is described in this paper. The model explains previously reported experimental studies related to the development of SP-based optical-fiber sensors. The method is based on a Fourier transform approach and predicts the appearance of a spatial SP resonance within the light diffracted from the waveguide edge. The approach also allows one to obtain the spectral dependence of light guided back from the remote waveguide edge and can be used to determine design parameters for optimum sensor operation.**

***Index Terms*— Aluminum, diffraction, gold, optical fiber, optical waveguide, slab waveguide, surface plasmon oscillations, surface plasmon resonance, thin film.**

I. Introduction

THE traditional prism coupling technique for observation of surface plasmon resonance (SPR) [1] has been used extensively in the literature for applications that include optical coating characterization [2], surface roughness determination [3], and chemical sensor development [4]. An optical-fiber configuration having the remote fiber tip polished at an angle relative to the fiber axis, with a value close to the SPR angle and coated with a 50-nm-thick film of either gold or silver was proposed in the literature [5] as a means of using the SPR transducing mechanism for the design of highly sensitive fiber probes for remote-sensing applications. A single-mode polished fiber probe coated with a 50-nm-thick silver film was later studied experimentally [6], with measurements of the polarization state of the backcoupled light exhibiting evidence of a SPR/effect on the metallized surface. Further experimental studies [7] indicated that the optical fiber could be configured to allow visual observation of a spatial SPR within the diffracted beam pattern coming out of the metallized probe.

In the work reported in this paper, a planar waveguide model is developed to account for the backcoupling [6] and diffraction effects [7] associated with SP oscillations excited on the metallized edge of the single-mode fiber. Theoretical results indicate that design parameters can be determined to allow developing planar-waveguide or single-mode optical-fiber versions of SPR-based remote-sensor systems.

Manuscript received December 10, 1997; revised December 10, 1997. This work was supported by the Conselho Nacional de Pesquisa-CNPQ, Brazil.

The author is with the Departamento de Electrônica e Sistemas, Universidade Federal de Pernambuco, Recife-PE, CEP: 50.740-530, Brazil.

Publisher Item Identifier S 0018-9480(98)02032-8.

II. SP Excitation in a Single-Mode Optical Fiber

The metallized optical-fiber configuration along with the experimental arrangement used previously to observe SPR effects is illustrated in Fig. 1 [7]. A polarizer is used to adjust the polarization state of the laser beam, which is focused to a single-mode fiber by use of lens $L1$. Lens $L2$ focuses a portion of the input beam to photodetector $PD1$ to allow one to obtain a reference signal. The portion of light directed to the single-mode fiber, mounted on a thin capillary tube, launches the fundamental propagating mode. The latter propagates along the fiber until reaching the polished end, coated with a 50-nm-thick gold film. The latter is used to allow coupling to a SP oscillation on the exposed surface. The polished portion of the fiber is illustrated in more detail in the expanded view shown in Fig. 1. The cylindrical cladding surface of the fiber tip is coated with a partially reflecting aluminum film. This enables part of the guided beam reflected from the gold-coated surface to diffract out of the capillary tube, with the light reflected from the aluminum film being partially coupled back to the fiber input after reflection on the gold-coated surface. The polishing angle α has a value close to that required for the onset of SP oscillations, which is approximately 45°, for the case of a silica–gold–air multilayer configuration [2]. The diffracted beam pattern is recorded by use of a 512-element photodiode array coupled to a 12-b analog-to-digital data acquisition system [7]. Because excitation of SP oscillations requires an E-field component perpendicular to the gold surface [1], the analyzer shown in Fig. 1 has to be adjusted for proper selection of the polarization state of the diffracted beam. Adjustment of the polarization state of the input beam can also provide the required E-field orientation on the gold surface, and this can be used to identify the resonance effect from the backcoupled light recorded by photodetector $PD2$.

Adjustment of the analyzer axis allowed identifying a spatial SPR effect as a dark strip of light within the diffracted light distribution, when the appropriate polarization state was selected [7]. Fig. 2 represents the digitally filtered TM light intensity distributions recorded with the photodetector array aligned along the largest beam dimension for two distinct wavelengths. In the inset of Fig. 1, a TM guided mode has H- and E-field components perpendicular and parallel to the incidence plane, respectively, the latter containing both the direction along the normal line to the metal surface and that along the fiber longitudinal axis. A TE wave would have

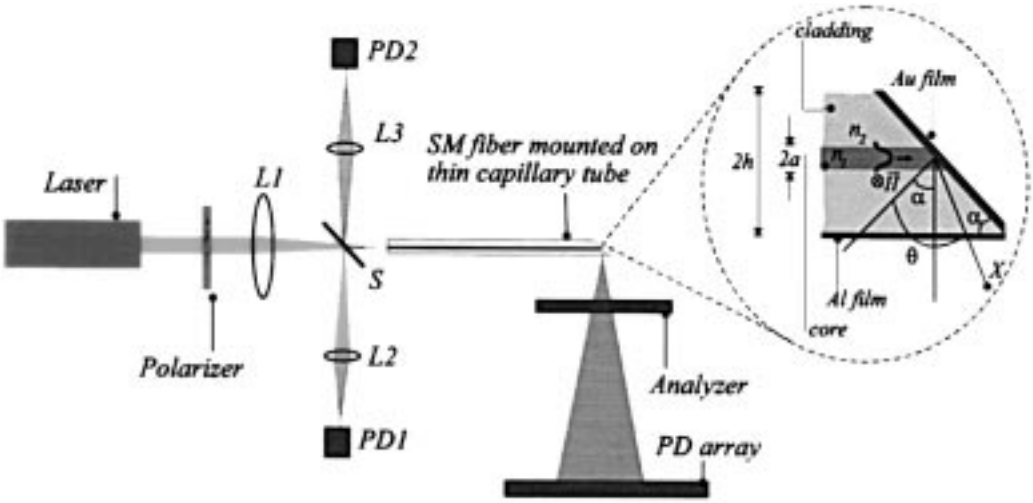

Fig. 1. Experimental arrangement to study the diffraction and backcoupling of SP oscillations on a metallized single-mode fiber probe [7].

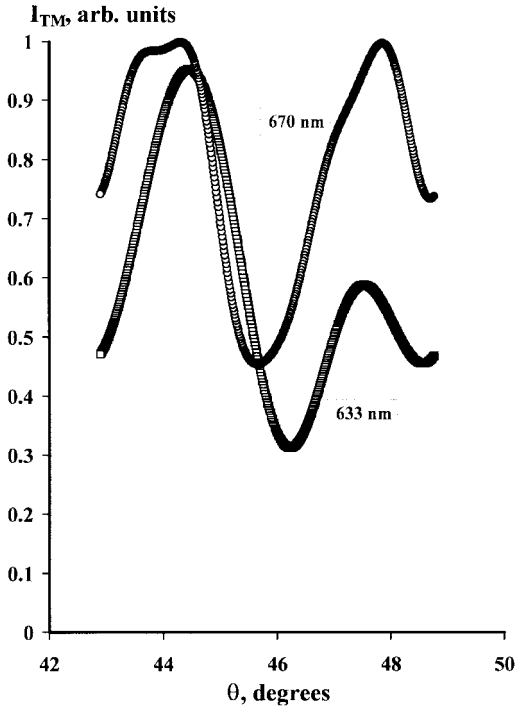

Fig. 2. SPR curves observed in the diffracted light out of a single-mode fiber for two wavelengths [7].

field components rotated 90° relative to those of the TM wave. The SP coupling effect is identified in the curves as a resonant absorption of the TM polarized light. No such effect was observed for TE polarized light in the work reported in [7]. Changing the light wavelength produced changes in resonance minimum position in agreement with experimental observations of SPR on a planar prism configuration; the latter exhibiting an upward shift of the minimum position for a downward shift in the driving wavelength [1].

Attempts to observe the SPR phenomenon from measurement of the ratio between orthogonal polarizations detected in the backcoupled light (as reported in the literature [6]) were not successful in [7], probably due to an unmatched value of the polishing angle α for the two probing wavelengths used in the experiments. The theoretical model described in the following sections, besides accounting for the experimental observations of the SPR effect present in the diffracted light distribution, allows selecting a proper polishing angle and probing wavelength for optimum observation of the SPR effect.

III. Theoretical Analysis

The fundamental features associated with the coupling of guided light with SP oscillations in a cylindrical fiber can be obtained from a simpler planar waveguide model. A guided mode in a slab waveguide is generally regarded to consist of a pair of plane waves reflecting back and forth at the core/cladding interface, each with a well-defined propagation angle relative to the longitudinal axis. Because the incidence angle θ_{SP} (for observation of the SPR, minimum intensity is set by the glass–gold–air multilayer structure) this interpretation could lead to the conclusion that a slight deviation of the angle α from the optimum value $\alpha_{\mathrm{opt}} = \pi/2 - \theta_{\mathrm{SP}}$ required to provide maximum coupling to the SP oscillation would frustrate observation of the SPR from the light distribution emanating from the metallized fiber tip. The existence of a spatial SPR resonance, as observed in [7], cannot be accounted for by this interpretation. One has instead to take into account that the guided mode is laterally confined in the waveguide. When the longitudinal waveguide structure is terminated at the polished surface, the transverse beam profile can be described in terms of a spatial Fourier spectrum. Each Fourier component corresponds to a plane wave striking the metal, each having a wave-vector component k parallel to the metal surface. The metal reflection coefficient represents the response of the surface to each of the plane-wave components, and is also a k-dependent parameter. Therefore, the metal reflection coefficient represents a filter function from which the beam, transmitted through the aluminum film, can be obtained.

This Fourier analysis can be extended to account for the amount of backcoupling and requires calculating the light distribution on the polished surface, after partial reflection from the thin aluminum film, illustrated in the expanded

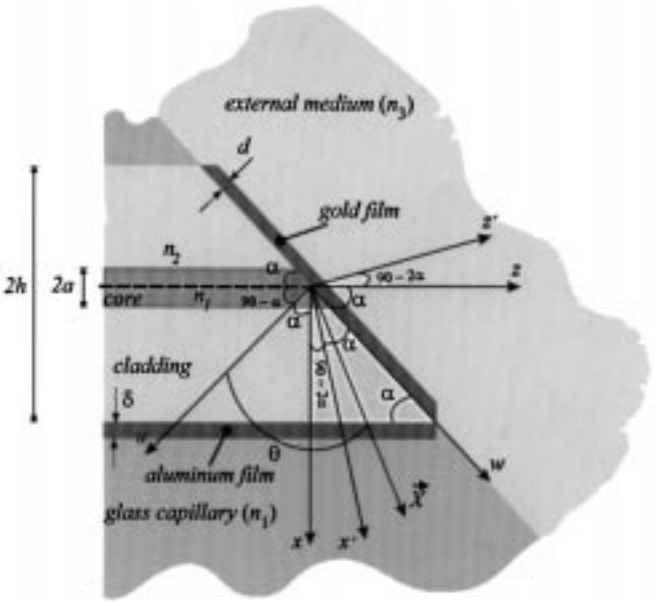

Fig. 3. Geometry employed for determination of diffraction and backcoupling of guided light in a planar waveguide.

view of Fig. 1. This light distribution is then filtered by the gold reflection function, after which it has to couple to the fundamental mode that will propagate back within the slab waveguide. In what follows, a detailed account for both light diffraction and backcoupling effects under SPR is described.

A. Slab Waveguide Edge Geometry and Fundamental Guided Modes

A shown in Fig. 3, the planar waveguide, having core and cladding thicknesses $2a$ and $2h$, respectively, is assumed to have one edge cut at an angle α. The core and cladding regions are assumed to have refractive indices n_1 and n_2, respectively. The end surface is coated with a metal film having a thickness d. Coordinate systems xz, $x'z'$, and uw, shown in Fig. 3, are defined relative to the edge of the metal surface with parameter θ defining the angle of the position vector $\overline{X}$ relative to the u-axis. Axes u and x define the normal directions to the gold and aluminum surfaces, respectively, and x' defines the specular direction relative to the waveguide longitudinal axis. Location of the gold–glass interface is defined by the condition $u = 0$ and that of the aluminum–cladding interface is defined by the condition $x = h$. The aluminum film is assumed to have thickness δ. To conform to the cylindrical fiber sensor configuration, the aluminum film is assumed to be covered by a medium representing the glass capillary and, therefore, having a refractive index close to that of silica.

Relationships between the several coordinates (shown in Fig. 3) can be obtained by use of the transformation matrix for a counterclockwise rotation of ϕ radians in the following plane:

$$\tilde{T}(\phi) = \begin{pmatrix} \cos\phi & \sin\phi \\ -\sin\phi & \cos\phi \end{pmatrix}. \tag{1}$$

For instance, the relationships between the xz- and the uw-systems can be written as

$$\tilde{X}_{xz} = \tilde{T}(\alpha)\tilde{X}_{uw} \tag{2}$$

$$\tilde{X}_{uw} = \tilde{T}(-\alpha)\tilde{X}_{xz} \tag{3}$$

where $\tilde{X}_{xz} \equiv \binom{x}{z}, \tilde{X}_{uw} \equiv \binom{u}{w}$.

Within the slab waveguide, either the H_y- or the E_y-field components associated, respectively, with the TM and TE guided modes propagating toward the end surface have coordinate dependence of the form [8]

$$\Psi_0^+(x,z) = \begin{cases} \cos(\beta_T x)e^{-j\beta z}, & \text{for } |x| \le a \\ e^{W}(\cos U)e^{-\gamma|x|}e^{-j\beta z}, & \text{for } |x| \ge a \end{cases} \tag{4}$$

with $U \equiv \beta_T a$, $W \equiv \gamma a$, $U^2 + W^2 = V^2$, and

$$V = (k_0 a)(n_1^2 - n_2^2)^{1/2} \tag{5}$$

where $k_0 = 2\pi/\lambda$, and λ is the free-space wavelength. The relationship between parameters U and W defines the dispersion relation for the TM and TE modes in the planar waveguide. Under the weakly guiding approximation, $n_1 \approx n_2$, yielding for both mode sets [8]

$$U \tan U \approx W. \tag{6}$$

B. Calculation of the Diffracted Light Intensity Distribution

To determine the light distribution exiting (the planar waveguide following reflection at the gold surface), we assume the weakly guiding condition $n_1 \approx n_2$ so that the confined beam can be represented as a Fourier integral of plane waves propagating in a medium of refractive index n_1. For a given plane wave having a wave-vector component k along the w-direction, the gold surface exhibits a reflection coefficient representative of the glass–gold film–outer medium multilayer structure. For a three-layer system comprising regions 1–3 with relative permittivities ε_1, ε_2, and ε_3, respectively, with regions 1 and 3 considered semi-infinite and with region 2 having thickness t, and assuming an input wave entering region 1, a generalization of the expressions given in the literature for the TM and TE reflectivities [1]–[3] can be obtained by use of the auxiliary function in (7), shown at the bottom of the page, with the Fresnel reflection R functions defined by

$$R_{\mathrm{TM}}(a,b,k) \equiv \frac{a(bk_0^2 - k^2)^{1/2} - b(ak_0^2 - k^2)^{1/2}}{a(bk_0^2 - k^2)^{1/2} + b(ak_0^2 - k^2)^{1/2}} \tag{8}$$

$$R_{\mathrm{TE}}(a,b,k) \equiv \frac{(bk_0^2 - k^2)^{1/2} - (ak_0^2 - k^2)^{1/2}}{(bk_0^2 - k^2)^{1/2} + (ak_0^2 - k^2)^{1/2}}. \tag{9}$$

Assuming the gold film having relative complex permittivity $\varepsilon_{\mathrm{Au}}$ and thickness d, in contact with the outer medium

$$\Gamma_{\mathrm{TM,TE}}(\varepsilon_1,\varepsilon_2,\varepsilon_3,t,k) = \frac{R_{\mathrm{TM,TE}}(\varepsilon_1,\varepsilon_2,k) + R_{\mathrm{TM,TE}}(\varepsilon_2,\varepsilon_3,k)\exp(-j2(\varepsilon k_0^2 - k^2)^{1/2}t)}{1 + R_{\mathrm{TM,TE}}(\varepsilon_1,\varepsilon_2,k)R_{\mathrm{TM,TE}}(\varepsilon_2,\varepsilon_2,k)\exp(-j2(\varepsilon k_0^2 - k^2)^{1/2}t)} \tag{7}$$

having refractive index n_3, as shown in Fig. 3, (8) and (9) allow expressing the TM and TE reflectivities at the waveguide–gold interface as $\Gamma_{\rm TM}(n_1^2, \varepsilon_{\rm Au}, n_3^2, d, k)$ and $\Gamma_{\rm TE}(n_1^2, \varepsilon_{\rm Au}, n_3^2, d, k)$, respectively.

In order to obtain the k-dependence of the plane-wave components of the guided beam at the gold surface, (2) is used to express the function given in (4) in terms of the uw-coordinates shown in Fig. 3, yielding

$$\Psi_0^+(u=0,w) \equiv f_0(w) = \begin{cases} \cos[\beta_T(\sin\alpha)w]e^{-j\beta(\cos\alpha)w}, \\ \qquad \text{for } |w| \le \dfrac{a}{\sin\alpha} \\ e^W(\cos U)e^{-\gamma(\sin\alpha)|w|}e^{-j\beta(\cos\alpha)w}, \\ \qquad \text{for } |w| \ge \dfrac{a}{\sin\alpha}. \end{cases} \tag{10}$$

In the calculations that follow, use is made of the integral transform equations for both the coordinate- and Fourier-space amplitudes

$$f(w) = \int_{-\infty}^{+\infty} F(k)\exp(-jkw)\,dk \tag{11}$$

$$F(k) = \frac{1}{2\pi}\int_{-\infty}^{+\infty} f(w)\exp(jkw)\,dw \tag{12}$$

with the auxiliary relation between incident and reflected k-space field amplitudes at an interface exhibiting a multilayer reflectivity $r_n(k)$ at the nth bounce

$$F_n(k) = r_n(k)F_{n-1}(k) \tag{13}$$

where F_{n-1} and F_n represent the k-space amplitudes before and after reflection, respectively. For the first reflection at the gold surface, $n = 1$.

The coordinate–space field amplitude after the first reflection at the gold surface and propagation out of the waveguide core can be calculated from (11) with a propagation factor attached to each plane-wave Fourier amplitude, yielding

$$f_1(u,w) = \int_{-\infty}^{+\infty} F_1(k)\exp(-jkw)\exp(-jqu)\,dk \tag{14}$$

where

$$k^2 + q^2 = n_1^2k_0^2. \tag{15}$$

To obtain the diffracted intensity distribution expected to be confined around the specular direction (defined by the x'-axis) wave vectors are first represented in the $x'z'$-system by use of the transformation matrix given in (1), yielding

$$\begin{pmatrix} q \\ k \end{pmatrix} = \tilde{T}[-(\pi/2-\alpha)]\begin{pmatrix} q' \\ k' \end{pmatrix}. \tag{16}$$

Substituting (16) into (14) yields

$$f_1(x',z') = \int_{-\infty}^{+\infty} F_1(q'\cos\alpha + k'\sin\alpha) \cdot \exp(-j\vec{K}\cdot\vec{X})\xi_1(k')\,dk' \tag{17}$$

with

$$q' = (n_1^2k_0^2 - k'^2 \tag{18}$$

$$\xi_1(k') \equiv \left(-\frac{k'}{q'}\cos\alpha + \sin\alpha\right) \tag{19}$$

$$\vec{K}\cdot\vec{X} = q'x' + k'z'. \tag{20}$$

In the far-field approximation [9], we assume the light distribution to be confined around the specular direction, which corresponds to the condition $k' \approx 0 \ll q'$. This allows the use of the following approximations in the kernel of (17):

$$\xi_1(k') = \left(-\frac{k'}{q'}\cos\alpha + \sin\alpha\right) \approx \sin\alpha$$

$$\vec{K}\cdot\vec{X} = q'x' + k'z' \approx \left(n_1k_0 - \frac{k'^2}{2n_1k_0}\right)x' + k'z'.$$

In addition, it is expected that most of the contribution to the light intensity observed at a given position vector $\vec{X}$ are originated by those wavelets having wave vector $\vec{K}$ closely parallel to that vector direction. Under this approximation, the argument of function F_1 in (17) can be put into the following form:

$$q'\cos\alpha + k'\sin\alpha \approx n_1k_0\frac{x'}{X}\cos\alpha + n_1k_0\frac{z'}{X}\sin\alpha.$$

Using the above approximations and the trigonometric relations obtained from Fig. 3, $z' = -X\cos(\alpha+\theta), x' = X\sin(\alpha+\theta)$, (17) can be expressed as

$$f_1(x',z') = (\sin\alpha)F_1[n_1k_0\sin\theta]\left(\frac{j2\pi n_1k_0}{X}\right)^{1/2} \cdot \exp(-jn_1k_0X) \tag{21}$$

yielding a cylindrical wave field distribution in the far field.

The Fourier component F_1 in (21) can be obtained by use of (13) with $n = 1$ and by determining F_0. The latter is obtained by calculating the Fourier integral of (10), as defined in (12). Even though this calculation requires a number of algebraic manipulations, it involves a straightforward computation of the Fourier transform of a combination of complex exponential terms. Carrying out this calculation, the diffracted light intensity distributions $I_{\rm TM}$ and $I_{\rm TE}$ produced by either the TM or TE modes are obtained by use of the appropriate reflectivities at the gold surface, yielding

$$I_{\rm TM,TE} = \frac{k_1}{2\pi X}(\sin\alpha)^2|\Gamma_{\rm TM,TE} \cdot [n_1^2, \varepsilon_{\rm Au}, n_3^2, d, n_1k_0\sin\theta]|^2|F_0[n_1k_0\sin\theta]|^2 \tag{22}$$

with $F_0(k) \equiv A(k) + B(k)$ and (23) and (24), shown at the bottom of the following page.

C. Calculation of the Back-Reflected Light Intensity

Calculation of the light intensity coupled back to the fiber input requires determination of the light distribution reflected back to the gold-coated surface after partial reflection from the thin aluminum film (see Fig. 3). The aluminum film is

assumed to have a thickness δ and relative complex permittivity $\varepsilon_{\mathrm{A1}}$ and is to be sandwiched between two identical semi-infinite regions with the same refractive index n_1. Under these conditions, the TM and TE aluminum reflectivities for a plane-wave component of the diffracted field with wave-vector component k_z parallel to the aluminum–cladding interface can be expressed by use of (7)–(9) as $\Gamma_{\mathrm{TM}}(n_1^2, \varepsilon_{\mathrm{A1}}, n_2^2, \delta, k_z)$ and $\Gamma_{\mathrm{TE}}(n_1^2, \varepsilon_{\mathrm{A1}}, n_2^2, \delta, k_z)$, respectively.

Using the matrix given in (1), wave vectors are transformed from the uw- to the xz-system by use of

$$\begin{pmatrix} q \\ k \end{pmatrix} = \tilde{T}(-\alpha)\begin{pmatrix} k_x \\ k_z \end{pmatrix}.$$

Using (14), the field at the aluminum front surface just prior to reflection can then be represented in the xz-system in the following form:

$$f_1(h,z) = \int F_1(k_x \sin\alpha + k_z \cos\alpha) \cdot \exp(-jk_x h)\exp(-jk_z z)\xi_2(k_z)\, dk_z \quad (25)$$

where

$$\xi_2(k_z) = \left(-\frac{k_z}{k_z}\sin\alpha + \cos\alpha\right). \quad (26)$$

Immediately after the $n = 2$ reflection at $x = h$, the k_z-dependent kernel in the integral of (25) has to be multiplied by the reflection coefficient $r_2(k_z)$ according to (13), yielding the following reflected field:

$$f_2(h,z) = \int r_2(k_z)F_1(k_x \sin\alpha + k_z \cos\alpha) \cdot \exp(-jk_x h)\exp(-jk_z z)\xi_2(k_z)\, dk_z. \quad (27)$$

The field given by (27) propagates toward the waveguide core and can be calculated by attaching the appropriate propagation factor to each plane-wave Fourier amplitude. Therefore, just prior to the $n = 3$ reflection at the gold surface, this field distribution, already expressed in the uw-system, is given by

$$f_2(u,w) = \int dk\{r_2(-q\sin\alpha + k\cos\alpha)F_1(k) \cdot \exp[-j2h(q\cos\alpha + k\sin\alpha)] \cdot \exp(jq''u)\exp(jk''w)\} \quad (28)$$

with

$$\begin{pmatrix} q'' \\ -k'' \end{pmatrix} \equiv \tilde{T}(2\alpha)\begin{pmatrix} q \\ k \end{pmatrix}. \quad (29)$$

By setting $u = 0$ and using the inverse transformation of (29), the field distribution immediately following the $n = 3$ reflection at the gold surface is obtained from (28) and expressed as

$$\begin{aligned} f_3(u=0,w) &= \int dk''\ \xi_3(k'')\{r_3(k'')r_2(q''\sin\alpha - k''\cos\alpha)r_1 \\ &\quad \cdot (q''\sin 2\alpha - k''\cos 2\alpha) \\ &\quad \times F_0(q''\sin 2\alpha - k''\cos 2\alpha) \\ &\quad \cdot \exp[-j2h(q''\cos\alpha + k''\sin\alpha)] \\ &\quad \cdot \exp(jk''w)\} \\ &\equiv \int dk''\ F_3(k'')\exp(jk''w) \end{aligned} \quad (30)$$

with

$$\xi_3(k'') = -\left(\frac{k''}{q''}\sin 2\alpha + \cos 2\alpha\right) \quad (31)$$

and $q'' = (n_1^2 k_0^2 - k''^2)^{1/2}$.

The reflected field distribution given by (30) couples to normal modes of the planar waveguide. To determine the amount of coupled light, the field distribution at the gold surface is assumed to be a combination of backward propagating guided modes Ψ_n^- within the waveguide in the following form:

$$f_3(u=0,w) = \sum_n \eta_n \Psi_n^-(u=0,w) \quad (32)$$

with the coupling coefficient η_n being obtained from the following projection:

$$\eta_n = \frac{1}{\int dw|\Psi_n^-(u=0,w)|^2} \cdot \int dw f_3(u=0,w)[\Psi_n^-(u=0,w)]^*. \quad (33)$$

Assuming single-mode operation, the coupling coefficient is determined by only considering propagation of the fundamental mode back to the waveguide input end. Because propagation occurs along the $-z$-direction, the corresponding field profile can be obtained from the complex conjugate of the forward mode given by (10) and, therefore,

$$\begin{aligned} [\Psi_0^-(u=0,w)]^* &= \Psi_0^+(u=0,w) \\ &= f_0(w) \\ &= \int dk\ F_0(k)\exp(-jkw). \end{aligned} \quad (34)$$

Setting $n = 0$ in (33) and using (34) yields

$$\eta_0 = \frac{1}{\int dw|f_0(w)|^2}\int dk'' \int dk\ F_3(k'')F_0(k) \cdot \int dw\ \exp[j(k''-k)w]. \quad (35)$$

$$A(k) = 2(\cos U)\frac{\gamma\sin\alpha\cos[(k-\beta\cos\alpha)a/\sin\alpha] - (k-\beta\cos\alpha)\sin[(k-\beta\cos\alpha)a/\sin\alpha]}{[(\gamma\sin\alpha)^2 + (k-\beta\cos\alpha)^2]} \quad (23)$$

$$B(k) = 2\frac{(k-\beta\cos\alpha)\cos U\sin[(k-\beta\alpha)a/\sin\alpha] - \beta_T\sin\alpha\sin U\cos[(k-\beta\cos\alpha)a/\sin\alpha]}{(k-\beta\cos\alpha)^2 - (\beta_T\sin\alpha)^2} \quad (24)$$

TABLE I
PARAMETERS REPRESENTATIVE OF THE EXPERIMENTAL CONDITIONS [7] AND USED IN THE NUMERICAL SIMULATIONS

Core thickness, $2a$	4 μm
Waveguide width, $2h$	125 μm
Core refractive index, n_1	1.46
Numerical aperture, NA	0.12
Gold film thickness, d	50 nm
Aluminum film thickness, δ	20 nm
Capillary glass refractive index, n_1	1.46
External medium refractive index, n_3	1

Carrying out the w-space integral yields

$$\eta_0 = \frac{2\pi}{\int dw|f_0(w)|^2} \int dk'' F_0(k'')F_3(k''). \tag{36}$$

The wave-vector components k'' and q'' can be expressed in terms of a single angular variable θ'' by use of the definitions $k'' \equiv n_1 k_0 \sin\theta''$, $q'' \equiv n_1 k_0 \cos\theta''$. Using (23), (24), and (30), the coupling coefficient for the TM and TE modes can be expressed as the ratio between an integral over the angular variable θ'' and the normalization factor, in the following form:

$$\begin{aligned}\eta_{\mathrm{TM,TE}} = {} & \frac{2\pi}{\int dw|f_0(w)^2} \int_{-\pi/2}^{\pi/2} d\theta'' \cos(2\alpha - \theta'') \\ & \cdot \{\Gamma_{\mathrm{TM,TE}}(n_1^2, \varepsilon_{\mathrm{Au}}, n_3^2, d, n_2 k_0 \sin\theta'')\Gamma_{\mathrm{TM,TE}} \\ & \cdot (n_1^2, \varepsilon_{\mathrm{Au}}, n_3^2, d, n_2 k_0 \sin(2\alpha - \theta'')) \\ & \times \Gamma_{\mathrm{TM,TE}}(n_1^2, \varepsilon_{\mathrm{A1}}, n_1^2, \delta, n_2 k_0 \sin(\alpha - \theta'')) \\ & \cdot F_0(n_1 k_0 \sin\theta'')F_0(n_1 k_0 \sin(2\alpha - \theta'')) \\ & \cdot e^{[-j2hn_1 k_0 \cos(\alpha - \theta'')]}\}. \end{aligned} \tag{37}$$

IV. RESULTS

Numerical calculations were carried out to determine the theoretical prediction for the diffraction and backcoupling effects associated with the SPR phenomenon. Parameter values used in the simulations are listed in Table I and are based on the experimental conditions adopted in [7]. As the calculations require determination of the parameters U and W for a given value of the V number, the auxiliary relation $U^2 + W^2 = V^2$ was used to express (6) in the following form:

$$V = U \sec U. \tag{38}$$

For both TM and TE modes, the maximum value of U is $\pi/2$. As the numerical simulations accounted for the spectral dependence of the diffraction and backcoupling effects within the range $0.5\ \mu\mathrm{m} \leq \lambda \leq 1\ \mu\mathrm{m}$, a cubic spline fit was used to represent the function $U = h(V)$, calculated from (38). Using this fitting procedure, the spectral dependence of the V number [as implied by (5)] could be taken into account to determine parameters U and W for an arbitrary value of the wavelength. In the simulations, the wavelength dispersion of the core and cladding refractive indices was neglected and, therefore, the waveguide numerical aperture NA, defined by the relation

$$\mathrm{NA} \equiv (n_1^2 - n_2^2)^{1/2}$$

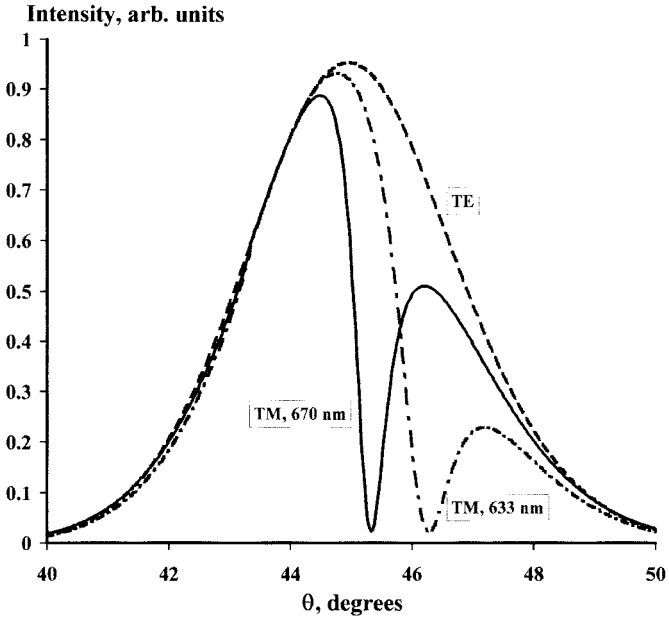

Fig. 4. Diffracted light distribution calculated from (22).

was assumed to remain constant within the wavelength range adopted for the calculations.

To account for the wavelength dependent SPR effect on the gold surface, optical constants of gold tabulated in the literature were used [10]. A cubic spline-fitting procedure was adopted to represent the gold data by a continuous wavelength-dependent function.

Fig. 4 shows the calculated diffracted light distribution for TE and TM polarizations obtained from (22) at the wavelengths of 633 and 670 nm, respectively. In these calculations, a constant value was assumed for the transmission factor through the aluminum film, as incorporation of this parameter would not cause any significant changes in the results. Notice that the SPR effect predicted by (22) is clearly observed for the TM polarization component and is absent for the TE polarization, in agreement with experimental observations [7]. A comparison of the plot of Fig. 4 with that of Fig. 2 indicates a good agreement for the resonance minimum positions. On the other hand, the curves shown in Fig. 2 are much broader and have a much smaller contrast than those depicted in Fig. 4. This departure of the experimental data relative to the theoretical prediction could be attributed to surface roughness on the gold-coated surface, as a result of the polishing procedure for construction of the fiber probe in the work conducted in [7]. This is a well-known effect (as reported in the literature [3]), affecting the dispersion relation of surface plasmon (SP) oscillations in thin-metal films.

Fig. 5 shows the wavelength dependence of the ratio between TM and TE mode intensities back-reflected to the waveguide input for two values of the polishing angle, namely, $\alpha = 45°$ and $46.5°$, as calculated from (37). In these calculations, a constant value was assumed for the aluminum reflectivity, as this function is expected to exhibit a rather small variation within the limits of the integral in (37).

Also shown in Fig. 5 are the expected resonance curves for the standard prism coupling configuration, calculated from the

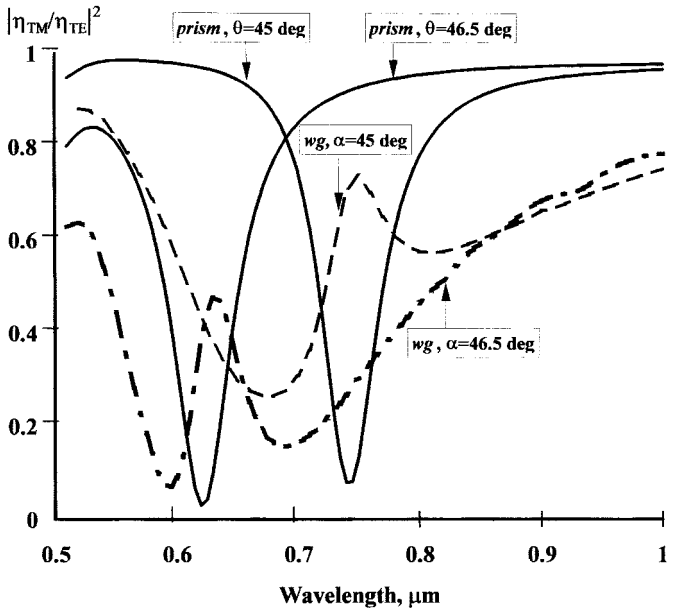

Fig. 5. Wavelength dependence of the ratio between TM and TE backcoupled intensities for two values of the polishing angle, as obtained from (37). Also plotted are the ratio curves between TM and TE reflectances for two values of the incidence angle, as calculated from the three-layer model.

following ratio:

$$r = \left| \frac{\Gamma_{\mathrm{TM}}(n_1, \varepsilon_{\mathrm{Au}}, 1, d, n_1 k_0 \sin\theta)}{\Gamma_{\mathrm{TE}}(n_1, \varepsilon_{\mathrm{Au}}, 1, d, n_2 k_0 \sin\theta)} \right|^2$$

assuming two values of the incidence angle, namely $\theta = 45°$ and $46.5°$, relative to the normal direction to the gold surface. The major difference of the SPR effect observed in a conventional prism coupling configuration relative to that under guiding is the appearance of double resonances. This is more striking when the calculated curve for $\alpha = 45°$ is compared to that corresponding to the prism configuration for $\theta = 45°$ where one would expect that the resonance effect under guiding would resemble that in the conventional prism coupling configuration. This would be so because for $\alpha = 45°$ the centermost portion of the forward propagating guided mode and the centermost portion of the diffracted beam, reflected from the aluminum surface, both reflect at the waveguide edge at the same angle of 45° relative to the normal direction to the gold surface.

The double resonance observed in Fig. 5 can be interpreted qualitatively by the simple picture of the guided mode being considered as a pair of plane waves bouncing back and forth at the core/cladding interface and propagating in directions slightly deviated from the waveguide axial direction. Under these conditions, there are effectively two distinct input angles that upon reflection from the gold surface would produce SPR minima located at distinct wavelengths. These minima would be shifted from that predicted by the standard three-layer model. It is interesting to notice that this point of view, although seeming satisfactory to explain the double resonance effect in the back-reflected light, cannot be used to describe the spatial resonance that is observed and predicted in (22) in the diffracted light.

The theoretical model can be extended to include the analysis of sensors built in a cylindrical fiber geometry. This would entail the use of a two-dimensional (2-D) Fourier transform to account for the field distribution of the guided and diffracted waves, as well as the inclusion of the vector nature of the fields into the formulation. For a cylindrical fiber, the absolute values of the backcoupling coefficients associated with the distinct polarizations are expected to be much smaller than those obtained for a slab waveguide geometry because in the former situation the diffracted beam spreads over a 2-D region on the polished surface, after being reflected back to the fiber core. However, because the TM backcoupling coefficient is only influenced by the SPR location within the wave-vector spread of the diffracted beam along the w-direction in Fig. 3 for a cylindrical fiber structure having the numerical aperture listed in Table I, one would expect that the ratio between TM and TE polarized light intensities would still exhibit resonances located very close to those calculated for the slab waveguide geometry, as shown in Fig. 5. Therefore, an examination of Fig. 5 indicates that optimum operating conditions for observation of the SPR effect from the backcoupled light, as a route to developing SPR-based systems for remote sensing either in a planar waveguide or in a single-mode fiber configuration, could be achieved for a polishing angle $\alpha = 46.5°$ and a setting wavelength $\lambda \approx 590$ nm.

V. Conclusions

A theoretical model that accounts for diffraction and backcoupling of SP oscillations at the metallized edge of a slab waveguide has been described. The model explains previously reported experimental observations of light diffraction under SPR in a single-mode optical fiber. Calculations of the spectral dependence of the back-reflected light intensities have indicated significant departures from the theoretical prediction that would be expected from the three-layer model used for determination of the SPR effect in the prism coupling scheme. It is expected that the theoretical model developed here can be useful for determination of optimum design parameters for using the SPR effect in waveguide or single-mode optical-fiber versions of SPR-based remote-sensor systems. Future work in this field should comprise experimental measurements of the spectral dependence of the back-reflection effect in both planar waveguide and single-mode optical-fiber configurations in order to confirm the validity of the theoretical model.

References

[1] E. Kretschmann, "Determination of optical constants of metals through the stimulation of surface plasma oscillations," (in German), *Z. Phys.*, vol. 241, pp. 313–324, 1971.

[2] W. P. Chen and J. M. Chen, "Use of surface plasma waves for determination of the thickness and optical constants of thin metallic films," *J. Opt. Soc. Amer.*, vol. 71, pp. 189–191, Feb. 1981.

[3] E. Fontana, "Analysis of optical surfaces by means of surface plasmon spectroscopy," *IEEE Trans. Instrum. Meas.*, vol. 45, pp. 399–405, Apr. 1996.

[4] M. T. Flanagan and R. H. Pantell, "Surface plasmon resonance and immunosensors," *Electron. Lett.*, vol. 20, no. 23, pp. 968–970, Nov. 1984.
[5] E. Fontana, "Surface plasma wave applications," Ph.D. dissertation, Elect. Eng. Dept., Stanford Univ., Stanford, CA, 1989, p. 128.
[6] L. de Maria, M. Martinelli, and G. Vegetti, "Fiber-optic sensor based on surface plasmon interrogation," *Sensors & Actuators B*, vol. 12, no. 3, pp. 221–223, Apr. 1993.
[7] E. Fontana, H. D. Dulman, R. H. Pantell, and D. E. Doggett, "Surface plasmon resonance on a single mode optical fiber," in *Proc. IEEE Instrum. Meas. Technol. Conf.*, Ottawa, Ont., Canada, May 1997, pp. 611–616.
[8] J. Singh, *Semiconductor Optoelectronics*, 1st ed. New York: McGraw-Hill, 1995, pp. 705–708.
[9] A. E. Siegman, *Lasers*, 1st ed. Stanford, CA: Univ. Sci. Books, 1986, p. 665.
[10] J. H. Weaver, "Optical properties of metals," in *Handbook of Chemistry and Physics*, 71st ed., D. R. Lide, Ed. Boston, MA: CRC Press, 1991, pp. 1287–1302.

Eduardo Fontana was born in Rio de Janeiro, Brazil, in 1957. He received the B.Sc. degree in electrical engineering and the M.Sc. degree in physics from the Federal University of Pernambuco, Pernambuco, Brazil, in 1980 and 1983, respectively, and the Ph.D. degree in electrical engineering from Stanford University, Stanford, CA, in 1989.

He is currently an Associate Professor in the Electronics and Systems Department, Federal University of Pernambuco. His past research activities have included microwave ferrite devices, low-temperature magnetic materials, magnetic semiconductors, optics, and free-electron lasers. His current research activities concern use of SP spectroscopy in thin-film technology, integrated optics devices, and the development of optical-fiber sensors.